states. If there are appreciable intermolecular interactions present between cations/anions/solvate molecules in the crystal of a $Fe^{II}Fe^{III}$(bimp) complex, then these interactions will tend to valence trap the complex. The complex will not have enough thermal energy to make an interconversion, overcoming interactions with neighboring molecules in the crystal. The sensitivity of this phenomenon is highlighted by the solvate molecule dependence observed for the $Fe^{II}Fe^{III}$(bimp) complexes. A solvate molecule is generally sitting in a crystal site near to the $Fe^{II}Fe^{III}$ cation. There are perhaps only weak van der Waals interactions; however they can be strong enough to valence trap the complex. As the crystal temperature is increased, the solvate–complex interaction weakens and in many cases the solvate molecules convert from being static to being dynamic. The $Fe^{II}Fe^{III}$(bimp) complex now finds itself in a more "pliable" environment in which it can make its large-amplitude motion necessary for the electron transfer.

The environmental sensitivity seen for the $Fe^{II}Fe^{III}$(bimp) complexes has implications for the iron–oxo $Fe^{II}Fe^{III}$ protein sites. These sites are likely very much influenced by the protein structure. Conformational changes of the protein, triggered off by substrate binding, docking with another protein, or configurational changes in the membrane to which the protein is attached, can have pronounced effects on the rate of electron transfer in the $Fe^{II}Fe^{III}$ protein site. This "environmental" sensitivity also provides an explanation for why the EPR signals for these $Fe^{II}Fe^{III}$ proteins are sensitive to whether the $Fe^{II}Fe^{III}$ protein form is prepared by either oxidizing the Fe_2^{II} protein or reducing the Fe_2^{III} protein.[43] The manner in which frozen solution protein sample is prepared for EPR studies, by slow or rapid cooling for example, could influence the appearance of the EPR signal.

Acknowledgment. This work was supported by the National Institutes of Health Grants HL13652 (D.N.H.) and GM45783, National Science Foundation Grant R11-8610671, and the Commonwealth of Kentucky through the Kentucky EPSCoR program (R.M.B.).

Supplementary Material Available: Tables of positional parameters, anisotropic thermal parameters, and hydrogen atom positional parameters and stereoplot of packing arrangement for $[Fe^{II}Fe^{III}(bimp)(O_2CPh)_2](BPh_4)_2 \cdot {}^3/_2CH_3CN$, table of Mössbauer spectra for $[Fe^{II}Fe^{III}(bimp)(O_2CCH_3)_2](ClO_4)_2 \cdot 2H_2O$, table of magnetic susceptibility for $[Fe^{II}Fe^{III}(bimp)(O_2CCH_3)_2](BF_4)_2$, figure of Mössbauer spectra for $[Fe^{II}Fe^{III}(bimp)(O_2CPh)_2](ClO_4)_2 \cdot 2H_2O$, electronic absorption spectrum of $[Fe^{II}Fe^{III}(bimp)(O_2CPh)_2](ClO_4)_2$ in CH_3CN, and cyclic voltammogram of $[Fe^{II}Fe^{III}(bimp)(O_2CPh)_2](ClO_4)_2$ in CH_3CN (21 pages); observed and calculated structure factors for $[Fe^{II}Fe^{III}(bimp)(O_2CPh)_2](BPh_4)_2 \cdot {}^3/_2CH_3CN$ (42 pages). Ordering information is given on any current masthead page.

Small Heteroborane Cluster Systems. 4. The Photochemistry and Organometallic Rearrangement Chemistry of Small Phosphorus-Bridged Borane Cluster Compounds: The Sequential Loss of Boron Vertices from Small Metallaboranes[1]

Bruce H. Goodreau, Lianna R. Orlando,† and James T. Spencer*

Contribution from the Department of Chemistry and the Center for Molecular Electronics, Center for Science and Technology, Syracuse University, Syracuse, New York 13244-4100.
Received May 16, 1991

Abstract: The photochemical decarbonylation and rearrangement of the small phosphorus-bridged, σ-metalated pentaborane(9) cluster $[Fe(\eta^5\text{-}C_5H_5)(CO)_2B_5H_7(\mu\text{-}P(C_6H_5)_2)]$ (**3**) was found to produce the organometallic tetraborane cluster complex $[Fe(\eta^5\text{-}C_5H_5)(CO)B_4H_6(P(C_6H_5)_2)]$ (**4**). The conversion of **3** to **4** was found to be accompanied by the loss of a carbonyl ligand from the iron fragment, the loss of a boron vertex from the cage, and a structural rearrangement to yield the new complex. The structure of complex **4** is based on a substituted *arachno*-pentaborane(11) parent cluster in which one of the BH_2 basal boron atoms has been replaced by an $Fe(\eta^5\text{-}C_5H_5)(CO)(\mu\text{-}PPh_2)$ fragment and a terminal *endo*-hydrogen on the opposite basal boron has been replaced by a diphenylphosphino group. The phosphine is also σ-bound to the iron center in a B–P–Fe bridged mode. Complex **4** was readily converted into the triborane complex $[Fe(\eta^5\text{-}C_5H_5)(CO)B_3H_7(P(C_6H_5)_2)]$ (**5**) through the loss of an additional vertex boron atom by passing **4** down a silica gel column. Both complexes **4** and **5** are relatively air stable materials. A single-crystal X-ray analysis of **5** shows that the structure is based on a substituted *arachno*-B_4H_{10} structure. An alternate description for **5** is based on a metalated $B_3H_8^-$ structure in which the iron fragment coordinates to one boron atom of the $B_3H_8^-$ ligand through a M–H–B interaction and the phosphorus atom bridges between the iron and the adjacent boron atom in much the same fashion as a bridging M–H–B hydrogen atom. Complex **5** represents the first structurally characterized metal triborane complex which exhibits a 1103 *styx* structure. The complete characterization by ^1H, ^{11}B, ^{13}C, ^{31}P NMR, infrared, and mass spectral analyses is reported. Crystallographic data for **5**: space group $P2_1/c$ (No. 14), a = 8.506 (1) Å, b = 14.127 (3) Å, c = 16.121 (3) Å, $\alpha = \gamma = 90.00°$, β = 102.73 (1)°, V = 1889.5 (6) Å^3, Z = 4 molecules/cell.

Introduction

Heteroborane and related heteroatom-bridged cluster compounds, especially the phosphorus-substituted systems, provide convenient models for a wide range of substituted polyhedral cluster systems including the other main group and transition-metal clusters. The relationship between the structures of these clusters and their organometallic chemistry has thus far not been explored in any detail. Very few studies in which the effect of

† National Science Foundation Research Experiences for Undergraduates Participant 1990–1992.

(1) Part 3: Goodreau, B. H.; Ostrander, R. L.; Spencer, J. T. *Inorg. Chem.* **1991**, *30*, 2066.

0002-7863/92/1514-3827$03.00/0

a heteroatom, such as phosphorus, on a small borane cage toward its reaction and organometallic chemistry have been reported. In this work we present the first detailed study of the organometallic reaction and photochemistry for a phosphorus-bridged borane cluster.

Stepwise cluster formation reactions and the inverse processes of cluster degradation are areas of intense current research interest. While numerous borane cage expansion reactions have been reported,[2-5] few reactions are known for the cage reduction process of a metallaborane in which a single boron vertex atom is removed.[5c,6,7] In one of the few known cage-reduction process, an apex BH unit is removed from a *closo*-($R_2C_2B_4H_4$)–transition-metal complex by the action of a Lewis base to form a *nido*-($R_2C_2B_3H_5$)–metal complex.[6] This reaction, while very useful for the preparation of intermediates for the synthesis of stacked organometallic–carborane sandwich compounds,[8] has not been extendable beyond the removal of a single vertex BH unit from the carborane cage. Finally, several cage reduction reactions have been reported for the large carborane clusters, such as the base-promoted reaction of *closo*-$C_2B_{10}H_{12}$ to form a *nido*-$C_2B_9H_{12}$ cluster.[2b] In this paper we report the first example of the sequential removal of boron atom vertices for a small phosphinoborane complex with the ultimate removal of two boron vertices. The application of this cage reduction reaction to related cluster systems may allow for the construction of new families of cluster complexes by stabilizing otherwise transient borane and heteroborane cages which can then be used as synthons for further cage reduction or expansion reactions.

The application of metallaborane compounds for the formation of metal boride thin film materials by chemical vapor deposition (CVD) is also an area of intense current interest.[9] In these deposition reactions, little is known about the mechanism of cage decomposition. Thus, an understanding of the organometallic cage rearrangement and reduction reations of discrete metallaborane species is therefore critical to the discovery of how these precursor compounds are involved in deposition processes.

Experimental Section

Physical Measurements. Boron (^{11}B) NMR spectra were recorded on a Cryomagnetics spectrometer operating at 80.26 MHz. Spectra were recorded in 5-mm tubes in both the ^1H coupled and decoupled modes and were externally referenced to BBr_3 at +40.0 ppm (positive chemical shifts indicate downfield resonances). The 2D $\{^1H\}^{11}B$-^{11}B COSY NMR spectra were obtained on a General Electric QE-500 spectrometer operating at 160.45 MHz. Carbon (^{13}C) NMR spectra were obtained on a General Electric QE-300 spectrometer operating at 75.48 MHz. The spectrometer was operated in the FT mode while locked on the deuterium resonance of the $CDCl_3$ solvent in 5-mm (o.d.) sample tubes. The reference was set relative to tetramethylsilane from the known chemical shifts of the $CDCl_3$ carbon atom. Phosphorus (^{31}P) NMR spectra were obtained in 5-mm (o.d.) tubes on a Cryomagnetics spectrometer operating at 101.27 MHz. Chemical shifts were referenced to an external standard of 85% phosphoric acid sealed in a 1-mm capillary tube. Both proton broad-band decoupled and coupled spectra were routinely observed for each sample with a decoupling power of about 5 W. Proton (^1H) NMR spectra were obtained on a General Electric QE-300 spectrometer operating at 300.15 MHz. Spectra were recorded on samples dissolved in $CDCl_3$ in 5-mm (o.d.) tubes with chemical shifts referenced to internal tetramethylsilane, with a positive shift indicating a resonance at a lower applied field than that of the standard. Unit resolution mass spectra were obtained on a Finnigan 4021 mass spectrometer using an ionization potential of either 18 or 20 eV. The high-resolution mass spectra were obtained on a VG Analytical 7035 magnetic sector mass spectrometer operating at 30 eV. FT-IR spectra in the range of 4000 to 400 cm^{-1} were measured on a Mattson Galaxy 2020 spectrometer and were referenced to the 1601.8-cm^{-1} band of polystyrene. All compounds were recorded as Nujol mulls sandwiched between KBr plates.

Materials. All solvents were reagent grade or better. THF and pentane were distilled from sodium metal/benzophenone under a dry nitrogen atmosphere prior to use. Methylene chloride was used as received after deoxygenation by bubbling dry nitrogen through the liquid and stored over 4-Å molecular sieves. $CDCl_3$ was degassed by repeated freeze–thaw cycles and finally stored in vacuo prior to use. Pentaborane(9) was taken directly from our laboratory stock. The [Fe(η^5-C_5H_5)$(CO)_2B_5H_7(P(C_6H_5)_2)$] (**3**) was prepared and purified by literature methods.[1] The photochemical conversion of **3** to **4** was carried out in a water-cooled reaction vessel with a quartz immersion well using broad band irradiation from a Conrad-Hanovia mercury vapor lamp (No. 7825-34). All other commercially available chemicals were used as received. Analytical thin-layer chromatography was conducted on 2.5 × 7.5 cm silica gel strips (1B-F, Baker) and conventional column chromatography was conducted using 20 cm columns packed with 230–400 mesh (ASTM) silica gel (EM Science).

[Fe(η^5-C_5H_5)$(CO)B_4H_6(P(C_6H_5)_2)$] (4). The photochemical reactor described above was charged with 2.00 g (4.73 mmol) of [Fe(η^5-C_5H_5)$(CO)_2B_5H_7(P(C_6H_5)_2)$] (**3**) and a dry nitrogen atmosphere was established. To the reactor was added 100 mL of freshly distilled and degassed THF. The solution was irradiated at room temperature for 7.5 h while maintaining constant stirring and the dry nitrogen atmosphere. During this time, the solution gradually changed from a clear yellow solution to a clear dark brown solution. The progress of the reaction was monitored periodically by ^{11}B NMR and FT-IR by the disappearance of reactant signals and the appearance of a new set of product signals along with small unidentified broad resonances. The photochemical conversion of complex **3** to **4** (as monitored by ^{11}B NMR) proceeds in 63.7% conversion. After the completion of the irradiation, the solvent was removed in vacuo and the residue extracted twice with 100 mL of pentane to produce a clear brown solution of a dark brown insoluble residue. The solution was filtered and the solvent removed to give 0.49 g of the product [Fe(η^5-C_5H_5)(CO)-$B_4H_6(P(C_6H_5)_2)$] (**4**) as a yellow solid in 27.6% isolated yield. The smaller isolated yield was due to the difficulties encountered in the isolation of pure **4** (achieved by repeated extractions) and the tendency of complex **4** to decompose. The product is relatively air-stable as a solid but shows significant decomposition after several hours of standing in solution open to the air. High-resolution electron-impact mass spectra: theoretical mass for $^{12}C_{18}{}^1H_{21}{}^{11}B_4{}^{56}Fe^{16}O^{31}P$ m/e 384.1051; measured mass m/e 384.1051. The 18-eV electron-impact mass spectrum of **4** exhibited the expected parent envelope region whose relative intensities corresponded with those calculated from the isotopic abundances of the elements in the structure as presented in Table II.[10] Two additional fragments were also prominent in the spectrum and were assigned to the parent fragment minus the carbonyl group and the loss

(2) (a) Onak, T. In *Comprehensive Organometallic Chemistry*; Wilkinson, G., Stone, F. G. A., Abel, E., Eds.; Pergamon: Oxford, 1982; Vol. 1, Chapter 5.4, p 411. (b) Reference 2a, p 428.

(3) Grimes, R. N. In *Comprehensive Organometallic Chemistry*; Wilkinson, G., Stone, F. G. A., Abel, E., Eds.; Pergamon: Oxford, 1982; Vol. 1, Chapter 5.5, p 485.

(4) Grebenik, P. D.; Leach, J. B.; Green, M. L. H.; Walker, N. M. *J. Organomet. Chem.* **1988**, *345*, C31.

(5) (a) Grebenik, P. D.; Green, M. L. H.; Kelland, M. A.; Leach, J. B.; Mountford, P. *J. Chem. Soc., Chem. Commun.* **1989**, 1397. (b) Grebenik, P. D.; Leach, J. B.; Pounds, J. M.; Mountford, P.; Green, M. L. H. *J. Organomet. Chem.* **1990**, *382*, C1. (c) Inkrott, K. E.; Shore, S. G. *J. Chem. Soc., Chem. Commun.* **1978**, 866. (d) Bown, M.; Greenwood, N. N.; Kennedy, J. D. *J. Organomet. Chem.* **1986**, *309*, C67. (e) Bould, J.; Greenwood, N. N.; Kennedy, J. D. *J. Chem. Soc., Dalton Trans.* **1982**, 481. (f) Gilbert, K. B.; Boocock, S. K.; Shore, S. G. In *Comprehensive Organometallic Chemistry*; Wilkinson, G., Stone, F. G. A.; Abel, E., Eds.; Pergamon: Oxford, 1982; Vol. 6, Chapter 41, p 879.

(6) (a) Spencer, J. T.; Grimes, R. N. *Organometallics* **1987**, *6*, 323. (b) Grimes, R. N.; Beer, D. C.; Sneddon, L. G.; Miller, V. R.; Weiss, R. *Inorg. Chem.* **1974**, *13*, 1138. (c) Maxwell, W. M.; Miller, V. R.; Grimes, R. N. *Inorg. Chem.* **1976**, *98*, 4818. (d) Swisher, R. G.; Sinn, E.; Grimes, R. N. *Organometallics* **1983**, *2*, 506. (e) Swisher, R. G.; Sinn, E.; Grimes, R. N. *Organometallics* **1985**, *4*, 890.

(7) (a) Venable, T. L.; Grimes, R. N. *Inorg. Chem.* **1982**, *21*, 887. (b) Miller, V. R.; Weiss, R.; Grimes, R. N. *J. Am. Chem. Soc.* **1977**, *99*, 5646. (c) Miller, V. R.; Grimes, R. N. *J. Am. Chem. Soc.* **1973**, *95*, 5078. (d) Peters, C. R.; Nordman, C. E. *J. Am. Chem. Soc.* **1960**, *82*, 5758. (e) Sneddon, L. G.; Voet, D. *J. Chem. Soc., Chem. Commun.* **1976**, 118. (f) Weiss, R.; Bowser, J. R.; Grimes, R. N. *Inorg. Chem.* **1978**, *17*, 1522.

(8) (a) Fessenbecker, A.; Stephan, M.; Grimes, R. N.; Pritzkow, H.; Zenneck, U.; Siebert, W. *J. Am. Chem. Soc.* **1991**, *113*, 3061. (b) Attwood, M. D.; Davis, J. H., Jr.; Grimes, R. N. *Organometallics* **1990**, *9*, 1177.

(9) (a) Dowben, P. A.; Spencer, J. T.; Stauf, G. T. *Mater. Sci. Eng. B* **1989**, *B2*, 297. (b) Amini, M. M.; Fehlner, T. P.; Long, G. J.; Politowski, M. *Chem. Mater.* **1990**, *2*, 432. (c) Zhang, Z.; Kim, Y. G.; Dowben, P. A.; Spencer, J. T. *Mater. Res. Soc. Symp. Proc.* **1989**, *131*, 407. (d) Glass, J. A., Jr.; Kher, S.; Hersee, S. D.; Ramseyer, G.; Spencer, J. T. *Mater. Res. Soc. Symp. Proc.* **1991**, *204*, 397. (e) Glass, J. A., Jr.; Kher, S.; Kim, Y.-G.; Dowben, P. A.; Spencer, J. T. *Mater. Res. Soc. Symp. Proc.* **1991**, *204*, 439. (f) Glass, J. A., Jr.; Kher, S.; Spencer, J. T. *Thin Solid Films* **1992**, *207*, 15. (g) Glass, J. A., Jr.; Kher, S.; Spencer, J. T. *Chem. Mater.* In press. (h) Kher, S.; Spencer, J. T. *Chem. Mater.* In press. (i) Lee, S.-W.; Li, D.; Dowben, P. A.; Perkins, F. K.; Onellion, M.; Spencer, J. T. *J. Am. Chem. Soc.* **1991**, *113*, 8444.

(10) Ditter, J. F.; Gerhart, F. J.; Williams, R. E. *Mass Spectroscopy of Inorganic Compounds* **1968**, 191, ACS Monogr. Ser. 7L.

Table I. NMR Data (ppm) for Phosphinoborane–Metal Complexes

compd	^{11}B Data[a]	^{1}H Data[b]	{^{1}H} ^{13}C Data[b]	^{31}P Data[c]
4[e]	30.2 (d, B(4), J_{BH} = 149 Hz), 25.7 (d, B(1), J_{BH} = 162 Hz), −21.2 (d, B(3), J_{BH} = 156 Hz), −29.6 (q, B(2), J_{BH} = 66 Hz, J_{BP} = 80 Hz)	−0.59 (br s, 1 H, B–H–B), 0.17 (br m, B–H terminal), 4.57 (s, 5 H, C_5H_5), 7.35 (m, 3 H, C_6H_5), 7.40 (m, 3 H, C_6H_5), 7.59 (m, 2 H, C_6H_5), 7.71 (m, 2 H, C_6H_5)	85.48 (s, C_5H_5), 132.12 (d, *o*-C_6H_5, J_{PC} = 8.9 Hz), 132.87 (d, *o*-C_6H_5, J_{PC} = 11.8 Hz), 128.06 (d, *m*-C_6H_5, J_{PC} = 7.0 Hz), 128.20 (d, *m*-C_6H_5, J_{PC} = 6.2 Hz), 128.66 (d, *p*-C_6H_5, J_{PC} = 3.7 Hz), 129.65 (d, *p*-C_6H_5, J_{PC} = 2.3 Hz), 129.08 (d, *i*-C_6H_5, J_{PC} = 10.1 Hz), 137.61 (d, *i*-C_6H_5, J_{PC} = 18.0 Hz), 201.75 (s, *C*O)	−10.1 (br)
5[e]	9.1 (s, B(3)), −24.5 (s[g], B(2), J_{BP} = 106 Hz[e]), −38.5 (s, B(1), J_{PBB} = 18 Hz[f])	−21.34 (br s, 1 H, Fe–H–B), −1.41 (br s, 1 H, B–H–B), 0.86 (br m, B–H terminal), 4.41 (s, 5 H, C_5H_5), 7.36 (m, 3 H, C_6H_5), 7.45 (m, 3 H, C_6H_5), 7.53 (m, 4 H, C_6H_5)		−11.8 (br)

[a] Relative to BBr_3 (40.0 ppm). Abbreviations: s = singlet, d = doublet, t = pseudotriplet (overlapping doublet of doublets), q = pseudoquintet (overlapping doublet of triplets), m = multiplet, unres = unresolved coupling, *o* = ortho, *m* = meta, *p* = para, *i* = ipso, br = broad. [b] Relative to TMS (0.0 ppm). [c] Relative to 85% H_3PO_4 (0.0 ppm). [d] In $CDCl_3$. [e] The broad singlet collapses into a phosphorus coupled doublet in the {^{1}H}^{11}B spectrum. [f] PB and PBB coupling constants determined from the 2D ^{11}B–^{11}B COSY NMR spectrum.

Table II. Infrared and Mass Spectral Data for Phosphinoborane–Metal Complexes

compd	IR data,[a] cm^{-1}	mass spectral data[b,c]
4	2565 (m, ν_{BH}), 2533 (m, ν_{BH}), 1948 (s, ν_{CO}), 1732 (m, $\nu_{\mu\text{-}BHB}$), 1261 (m), 802 (m), 740 (m), 694 (w)	386 (found 2.7, calcd 2.6; P$^+$ envelope), 385 (found 17.2, calcd 20.8; P$^+$ envelope), 384 (found 91.7, calcd 100; P$^+$ envelope, $^{12}C_{18}{}^{1}H_{21}{}^{11}B_4{}^{56}Fe^{16}O^{31}P$), 383 (found 100.0, calcd 88.8; P$^+$ envelope), 382 (found 60.3, calcd 37.6; P$^+$ envelope), 381 (found 16.7, calcd 10.6; P$^+$ envelope), 380 (found 6.7, calcd 2.3; P$^+$ envelope), 356 (100.0, P$^+$ − CO envelope), 276 (25.4, P$^+$ − P(C_6H_5) envelope)
5	2531 (m, ν_{BH}), 2504 (m, ν_{BH}), 2475 (w, ν_{BH}), 1962 (s, ν_{CO}), 1302 (w), 1262 (w), 1098 (m), 801 (w), 741 (m), 696 (w), 575 (m), 556 (w), 513 (w)	374 (found 100, calcd 100; P$^+$ envelope, $^{12}C_{18}{}^{1}H_{22}{}^{11}B_3{}^{56}Fe^{16}O^{31}P$), 373 (found 86.1, calcd 68.6; P$^+$ envelope), 372 (found 85.3, calcd 22.4; P$^+$ envelope), 371 (found 53.7, calcd 5.6; P$^+$ envelope), 346 (31.6, P$^+$ − CO), 186 (100, Fe(η^5-$C_5H_5)_2^+$)

[a] KBr plates. Abbreviations: vs = very strong, s = strong; m = medium; w = weak; sh = shoulder; br = broad. [b] Relative intensities are given with the largest peak in the envelope normalized to 100.0%. The calculated values are based on the natural isotopic abundances of the elements[10] which are normalized to the most intense peak in the envelope. [c] The spectrum for compound **4** was measured at 18 eV and that for compound **5** was measured at 20 eV.

of a P(C_6H_5) fragment. The fragmentation pattern clearly shows the presence of P($C_6H_5)_2$ and Fe(CO)(η^5-C_5H_5) fragments. The spectroscopic characterization of **4** is given in Tables I and II.

[Fe(η^5-C_5H_5)(CO)B_3H_7(P($C_6H_5)_2$)] (5). A 2-mL CH_2Cl_2 solution containing 0.071 g (0.18 mmol) of **4** was chromatographed on a 2 × 20 cm silica gel column and eluted with a 1:1 CH_2Cl_2:pentane solution. A deep orange-colored band (R_f in 10% CH_2Cl_2/pentane = 0.94 and travelled at the solvent front in 50% CH_2Cl_2/pentane) slowly developed from an initially yellow-colored band of complex **4**. The orange band was collected and the solvent removed in vacuo to yield 0.019 g of pure [Fe(η^5-C_5H_5)(CO)B_3H_7(P($C_6H_5)_2$)] (**5**) in 27.8% isolated yield as a dark orange solid. Compound **5** is a relatively air stable compound although significant decomposition was observed on standing in solution open to the air. High-resolution electron-impact mass spectra: theoretical mass for $^{12}C_{18}{}^{1}H_{21}{}^{11}B_4{}^{56}Fe^{16}O^{31}P$ *m/e* 374.103; measured mass *m/e* 374.109. The spectroscopic characterization of compound **5** is given in Tables I and II.

X-ray Crystallography of 5. A triangular, wedge-shaped, dark orange crystal of [($C_6H_5)_2PB_3H_7$Fe(η^5-C_5H_5)(CO)] (**5**), with approximate dimensions of 0.30 × 0.10 × 0.05 mm, was grown from a saturated 30% methylene chloride in pentane solution by slow solvent evaporation. The crystal was mounted in a 0.3-mm Lindemann capillary tube and sealed under an inert atmosphere. All measurements were made on a Rigaku AFC5S diffractometer using graphite monochromated Mo Kα radiation (λ = 0.71073 Å). Cell constants and an orientation matrix for the data collection were obtained from a least-squares refinement using 25 centered high-angle reflections in the range of 26.11° < 2θ < 29.90°. On the basis of the systematic absences of *h*0*l* for $l \neq 2n$ and 0*k*0 for $k \neq 2n$ and the successful structural solution, the space group was uniquely determined to be $P2_1/c$ (No. 14). Data were collected at room temperature using a ω–2θ scan technique. Three reference reflections were monitored every 150 reflections during data collection with no intensity loss observed during the collection. Crystallographic data for this compound are presented in Table III.

Data reduction of the 4833 measured reflections resulted in 4532 unique reflections (R_{int} = 0.146). After the application of corrections for Lorentz and polarization effects, 2422 independent reflections with $I > 3\sigma(I)$ were obtained which were used for the structure refinement

Table III. Crystallographic Data for [($C_6H_5)_2PB_3H_7$Fe(η^5-C_5H_5)(CO)] (**5**)

chem formula	$C_{18}H_{22}B_3FeOP$	diffractometer	Rigaku AFC5S
fw	373.62		
cryst system	monoclinic	ρ_{calcd}, g cm^{-3}	1.313
space group	$P2_1/c$ (No. 14)	μ, cm^{-1}	8.80
temp, K	298	transm coeff	
cell dimens		Ψ	0.9041–1.0000
(at 298 K)		Ψ_{av}	0.9687
a, Å	8.506 (1)	*R*, %	3.9
b, Å	14.127 (3)	R_w, %	4.1
c, Å	16.121 (3)	tot no. of reflcn	4833
α, deg	90.00	no. of reflcns	2422
β, deg	102.73 (12)	with $I > 3\sigma(I)$	
γ, deg	90.00	no. of variables	305
V, Å^3	1889.5 (6)	$2\theta_{max}$, deg	55.0
Z, molecules/cell	4	goodness of fit	1.30
		max shift/error	0.03
λ(Mo Kα), Å	0.71073	in final cycle	

(reflection/parameter = 7.94). Azimuthal scans of several reflections indicated that an absorption correction was not required. The position of the iron atom was determined from a Patterson synthesis and the remaining non-hydrogen atoms were located by application of direct methods to generate a trial structure.[11,12] The non-hydrogen atoms were refined anisotropically. All the hydrogen atoms were then located on a difference map and were refined isotropically. The final cycle of a full-matrix least-squares refinement converged with $R = \sum||F_o| - |F_c||/\sum|F_o| = 0.039$ and $R_w = [(\sum w(|F_o| - |F_c|)^2/\sum w(F_o)^2)]^{1/2} = 0.041$. The function minimized was $\sum w(|F_o| - |F_c|)^2$ (where $w = 4F_o{}^2/s^2(F_o{}^2)$, $s^2(F_o{}^2) = [S^2(C + R^2B) + (pF_o{}^2)^2]Lp^2$).[13] Plots of $\sum w(|F_o| - |F_c|)^2$

(11) Calbrese, J. C., PHASE—Patterson Heavy Atom Solution Extractor. University of Wisconsin–Madison, Ph.D. Thesis, 1972.

(12) Beurskens, P. T., DIRDIF: Direct Methods for Difference Structures. Technical Report 1984/1; Crystallography Laboratory, Toernooiveld, 6525 Ed. Nijmegen, The Netherlands.

Scheme I. The Deprotonation and Organometallic Reaction Chemistry of Bridging Diphenylphosphinopentaborane[a]

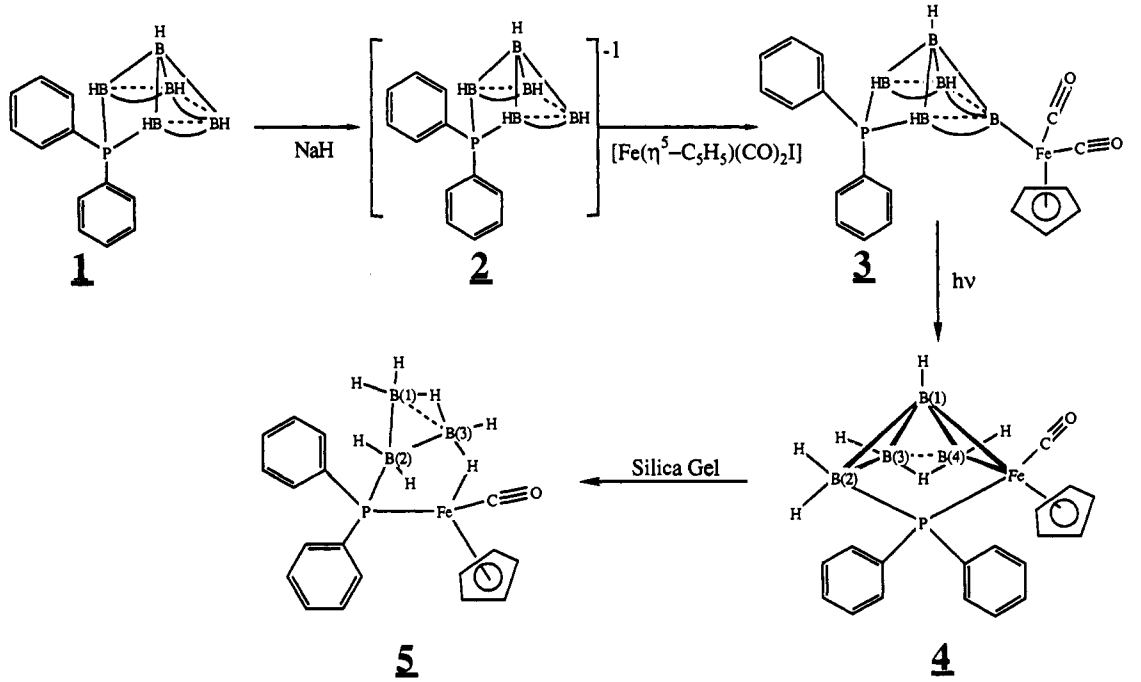

[a] Curved bonds indicate a bridging hydrogen atom.

Table IV. Positional Parameters and B(eq) for $[Fe(\eta^5\text{-}C_5H_5)(CO)B_3H_7P(C_6H_5)_2]$ (**5**)[a]

atom	x	y	z	B(eq), Å^2
Fe	0.58133 (6)	0.29548 (4)	0.75435 (3)	2.49 (2)
P	0.6372 (1)	0.22184 (6)	0.87826 (6)	2.22 (4)
O(1)	0.4712 (4)	0.1258 (2)	0.6576 (2)	5.5 (2)
C(1)	0.5117 (5)	0.1916 (3)	0.6980 (2)	3.4 (2)
C(2)	0.8094 (5)	0.3506 (3)	0.7670 (3)	4.0 (2)
C(3)	0.7067 (6)	0.4215 (3)	0.7855 (3)	3.9 (2)
C(4)	0.5869 (6)	0.4358 (3)	0.7120 (3)	4.2 (2)
C(5)	0.6128 (7)	0.3747 (4)	0.6496 (3)	4.6 (2)
C(6)	0.7523 (7)	0.3213 (4)	0.6843 (4)	4.7 (2)
C(7)	0.7405 (4)	0.1080 (2)	0.8825 (2)	2.3 (1)
C(8)	0.7309 (5)	0.0423 (3)	0.9456 (3)	3.2 (2)
C(9)	0.8060 (5)	−0.0454 (3)	0.9470 (3)	3.8 (2)
C(10)	0.8884 (5)	−0.0679 (3)	0.8865 (3)	4.2 (2)
C(11)	0.9003 (5)	−0.0027 (3)	0.8248 (3)	4.2 (2)
C(12)	0.8250 (5)	0.0838 (3)	0.8222 (3)	3.4 (2)
C(13)	0.7652 (4)	0.2903 (3)	0.9632 (2)	2.7 (1)
C(14)	0.9302 (5)	0.2757 (3)	0.9860 (3)	3.8 (2)
C(15)	1.0267 (7)	0.3330 (4)	1.0468 (3)	5.5 (3)
C(16)	0.9601 (9)	0.4035 (4)	1.0862 (4)	6.2 (3)
C(17)	0.7991 (8)	0.4177 (4)	1.0643 (3)	5.7 (3)
C(18)	0.7000 (6)	0.3621 (3)	1.0036 (3)	4.2 (2)
B(1)	0.3489 (6)	0.3059 (4)	0.8281 (4)	4.1 (2)
B(2)	0.4262 (5)	0.2125 (4)	0.9030 (3)	3.1 (2)
B(3)	0.2416 (6)	0.2000 (5)	0.8230 (4)	5.1 (3)
H(1)	0.413 (4)	0.317 (2)	0.771 (2)	3.3 (8)
H(1B)	0.342 (4)	0.370 (3)	0.862 (2)	4 (1)
H(2B)	0.224 (5)	0.293 (3)	0.795 (3)	6 (1)
H(3B)	0.146 (5)	0.194 (3)	0.855 (3)	6 (1)
H(4B)	0.233 (4)	0.162 (2)	0.760 (2)	3.7 (9)
H(5B)	0.389 (5)	0.143 (3)	0.884 (3)	6 (1)
H(6B)	0.420 (4)	0.230 (3)	0.969 (2)	4 (1)

[a] The positional and B(eq) data for the (C_6H_5) and (C_5H_5) protons are available in the supplementary material.

versus $|F_o|$, reflection order in data collection, sin θ/λ, and various classes of indices showed no unusual trends. The weighting scheme was based on counting statistics and included a factor (p = 0.03) to downweight intense reflections. Atomic scattering factors were from Cromer and Waber.[14] Terms for anomalous scattering were included in F_{calc}[15] and used the values for $\Delta f'$ and $\Delta f''$ previously reported.[13] The maximum and minimum peaks on the final difference Fourier map corresponded to 0.45 and −0.26 e$^-$/Å^3, respectively. Final atom coordinates and B(eq) are given in Table IV. A full tabular presentation of crystallographic data, including complete tables of intramolecular and intermolecular bond distances and angles, anisotropic thermal parameters, all atom coordinates including all hydrogen atoms, and a listing of observed and calculated structure factors is available as supplementary material.

The final structure was plotted using the TEXSAN[16a] graphics programs including PLUTO[16b] and ORTEP.[16c] Figures 3 and 4 show the molecular drawings of **5** with the atom labeling scheme indicated. Selected bond

Table V. Selected Intramolecular Bond Angles (deg) for $[Fe(\eta^5\text{-}C_5H_5)(CO)B_3H_7P(C_6H_5)_2]$ (**5**)[a]

P–Fe–C(1)	93.1 (1)	H(4B)–B(3)–B(1)	112 (4)
P–Fe–H(1)	87 (1)	H(4B)–B(3)–B(2)	124 (2)
C(1)–Fe–H(1)	92 (1)	B(3)–H(5B)–B(2)	82 (2)
O(1)–C(1)–Fe	175.8 (4)	H(5B)–B(3)–B(2)	35 (2)
Fe–H(1)–B(1)	136 (2)	H(5B)–B(2)–P	104 (2)
H(1)–B(1)–B(2)	117 (2)	H(5B)–B(2)–B(3)	63 (2)
H(1)–B(1)–B(3)	114 (2)	H(5B)–B(2)–B(1)	116 (2)
H(1)–B(1)–H(1B)	112 (3)	H(5B)–B(2)–H(6B)	115 (3)
H(1)–B(1)–H(2B)	103 (3)	H(6B)–B(2)–P	115 (2)
H(1B)–B(1)–H(2B)	103 (3)	H(6B)–B(2)–B(1)	113 (2)
H(1B)–B(1)–B(2)	109 (2)	H(6B)–B(2)–B(3)	119 (2)
H(1B)–B(1)–B(3)	132 (2)	B(1)–B(2)–B(3)	57.6 (3)
B(1)–H(2B)–B(3)	89 (2)	B(2)–B(3)–B(1)	61.3 (3)
H(2B)–B(1)–B(2)	112 (2)	B(2)–B(1)–B(3)	61.1 (3)
H(2B)–B(3)–B(1)	39 (2)	B(2)–P–Fe	101.2 (1)
H(2B)–B(3)–H(3B)	101 (3)	B(2)–P–C(7)	113.2 (2)
H(2B)–B(3)–H(4B)	101 (3)	B(2)–P–C(13)	108.0 (2)
H(2B)–B(3)–B(2)	99 (2)	C(7)–P–C(13)	103.6 (2)
H(3B)–B(3)–H(4B)	119 (3)	C(7)–P–Fe	117.1 (1)
H(3B)–B(3)–B(1)	120 (2)	C(13)–P–Fe	113.7 (1)
H(3B)–B(3)–B(2)	107 (2)		

[a] Estimated standard deviations in the least significant figure are given in parentheses.

(13) Cromer, D. T.; Waber, J. T. *International Tables for X-ray Crystallography*; Kynoch: Birmingham, England, 1974; Vol. IV, Table 2.3.1.

(14) Cromer, D. T.; Waber, J. T. *International Tables for X-ray Crystallography*; Kynoch: Birmingham, England, 1974; Vol. IV, Table 2.2A.

(15) Ibers, J. A.; Hamilton, J. T. *Acta Crystallogr.* **1964**, *17*, 781.

(16) (a) TEXSAN—Texray Structure Analysis Package, Molecular Structure Corp., 1985. (b) Motherwell, S.; Clegg, W. PLUTO. Program for plotting molecular and crystal structures. University of Cambridge, England, 1978. (c) Johnson, C. K., ORTEPII. Report ORNL-5138. Oak Ridge National Laboratory, Oak Ridge, TN, 1976.

Table VI. Selected Intramolecular Bond Distances (Å) for $[Fe(\eta^5\text{-}C_5H_5)(CO)B_3H_7P(C_6H_5)_2]$ (**5**)[a]

Fe–P	2.209 (1)	B(2)–B(3)	1.807 (7)
Fe–C(1)	1.758 (4)	B(1)–H(1)	1.18 (3)
Fe–C(2)	2.058 (4)	B(1)–H(1B)	1.07 (4)
Fe–C(3)	2.080 (4)	B(1)–H(2B)	1.09 (4)
Fe–C(4)	2.100 (4)	B(1)–H(6B)	2.47 (4)
Fe–C(5)	2.092 (5)	B(2)–H(6B)	1.11 (4)
Fe–C(6)	2.061 (4)	B(2)–H(5B)	1.05 (4)
Fe–H(1)	1.54 (3)	B(3)–H(2B)	1.38 (4)
Fe–B(1)	2.525 (5)	B(3)–H(3B)	1.06 (4)
Fe–B(2)	3.202 (4)	B(3)–H(4B)	1.13 (4)
Fe–B(3)	3.578 (5)	B(3)–H(5B)	1.62 (4)
P–C(7)	1.827 (3)	C(7)–C(8)	1.392 (5)
P–C(13)	1.827 (4)	C(8)–C(9)	1.391 (5)
P–B(1)	2.684 (5)	C(9)–C(10)	1.359 (6)
P–B(2)	1.928 (4)	C(10)–C(11)	1.375 (6)
P–B(3)	3.300 (5)	C(11)–C(12)	1.377 (5)
O(1)–C(1)	1.144 (5)	C(12)–C(7)	1.374 (5)
C(2)–C(3)	1.404 (6)	C(13)–C(14)	1.386 (5)
C(3)–C(4)	1.398 (6)	C(14)–C(15)	1.390 (6)
C(4)–C(5)	1.379 (7)	C(15)–C(16)	1.370 (8)
C(5)–C(6)	1.414 (7)	C(16)–C(17)	1.352 (8)
C(6)–C(2)	1.379 (7)	C(17)–C(18)	1.386 (7)
B(1)–B(2)	1.812 (7)	C(18)–C(13)	1.386 (5)
B(1)–B(3)	1.744 (9)		

[a] The estimated standard deviations in the least significant figure are given in parentheses.

angles and bond lengths are given in Tables V and VI, respectively.

Results and Discussion

The photochemical reaction of the bridged phosphinopentaborane–iron complex **3**, shown in Scheme I, produces the new metallapentaborane complex **4**. This conversion is accompanied by the loss of a carbonyl ligand from the iron fragment, the loss of a boron vertex from the cage, and a structural rearrangement to yield the new complex. The subsequent reaction of compound **4** with silica gel was found to convert it into the new complex **5** through the loss of an additional vertex boron atom and a second structural rearrangement. This final structural rearrangement appears to be less severe than that required for the formation of **4**. While many borane and metallaborane cage expansion (aufbau)[5d] processes are known,[2a,3,4] including photochemical expansion reactions,[5a] few reactions have been reported for the removal of a single boron vertex atom[2b,5c,6,7a] from a small metallaborane cluster and none in which this process has been carried out sequentially to remove two vertices. The spectroscopic data for the new compounds reported in this paper are presented in Tables I and II.

The proposed structure for complex **4**, shown in Scheme I, is that of a substituted *arachno*-pentaborane(11) system in which one of the BH_2 basal boron units has formally been replaced by an $Fe(\eta^5\text{-}C_5H_5)(CO)(\mu\text{-}PPh_2)$ fragment and a terminal *endo*-hydrogen on the opposite basal boron has been replaced by a terminally bound diphenylphosphino group which is, in turn, bound to the iron center. In addition, the bridging proton located between the B(2) and B(3) atoms in the *arachno*-B_5H_{11} parent structure has shifted to occupy a terminal position on B(2), thus formally creating a BH_2L group (where L is the PPh_2Fe group). Finally, the bridging proton between B(4) and the B(5) iron occupied site is not present. The complex possesses overall electroneutrality and may possess some zwitterionic character with a partial positive charge located on the exopolyhedral phosphorus atom and a partially negative charge delocalized over the entire ferraborane cage. This type of polarization is similar to that found for the triphenylphosphinomethyl derivative of the triborane ligand, $[(C_6H_5)_3PCH_2B_3H_7]$, in which a quaternary phosphino group is linked to the triborane ring through a methylene unit.[17] The increase in the charge localization on phosphorus is consistent with the observed downfield ^{31}P NMR chemical shift of **4** relative to the phosphorus center in the starting complex **3** ($\Delta\delta$ = +42.2 ppm). The ^{31}P NMR chemical shift of **4** (δ = −10.1 ppm) is also very near the range typically observed for quartenary phosphonium compounds (δ = 0 to +25 ppm).[18] The resonance in **4** has been shifted to slightly more negative values presumably by borane ring resonance effects. The absence of a M–H–B bridging proton was confirmed in the ^1H NMR spectrum in which a resonance for a typical M–H–B proton (δ = −5 to −20 ppm) was not observed over the range of temperatures from −60 °C to room temperature.

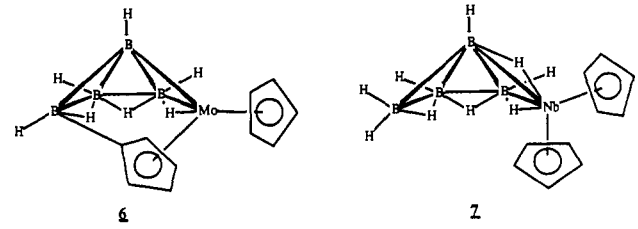

6 **7**

Figure 1. Structures of complexes **6** and **7**.

Several structurally related metallapentaborane species based on a substituted *arachno*-B_5H_{11} parent structure have been recently reported in the literature and include $[Mo(\eta^5\text{-}C_5H_5)(\eta^5{:}\eta^1\text{-}C_5H_4)B_4H_7]$[5a] (**6**), $[Nb(\eta^5\text{-}C_5H_5)_2B_4H_9]$[5b] (**7**), $[1\text{-}(C_6Me_6)\text{-}MHB_4H_9]$ (where M = Ru or Os)[5d] (**8**), and $[L(CO)IrB_4H_9]$ (where L = Me_3P or $PhMe_2P$).[5e,f] The molybdenum complex **6** was prepared by a photochemically induced cage building process from the reaction of $[Mo(\eta^5\text{-}C_5H_5)_2B_2H_6]$ with BH_3·THF while the other complexes were prepared from the direct interaction of either a borane cage or its corresponding anion with an appropriate organometallic reactant, such as $[(\eta^6\text{-}C_6H_6)MCl_2]$[5d] or $[(\eta^5\text{-}C_5H_5)_2MH_3]$.[5b] In all of these complexes derived from the *arachno*-B_5H_{11} parent structure, the metal substituent occupies the apical position in the cage except in the cases of complexes **6** and **7**. The X-ray crystal structure of complex **6**, shown diagramatically in Figure 1, is based on an *arachno*-B_5H_{11} parent structure in which a basal boron vertex is replaced with a $Mo(\eta^5\text{-}C_5H_5)(\eta^5{:}\eta^1\text{-}C_5H_4)$ fragment and one of the cyclopentadienyl protons of the $Mo(\eta^5\text{-}C_5H_5)_2$ unit is replaced by a boron–carbon σ-bond subrogating the *endo*-terminal proton on the parent structure. The NMR data reported for **6** are similar to those observed for compound **4**. In the case of complex **6**, however, the bridging proton between the B(2) and B(3) atoms of the parent *arachno*-B_5H_{11} structure does not shift out to occupy a terminal position as in complex **4** but remains in a bridging position. This behavior is anticipated on the basis of both theoretical and spectroscopic studies which have shown that the weaker the Lewis base strength of the ligand attached to the cage, the greater is the preference of the compound to adopt an asymmetric structure in which a proton has shifted from a bridging to a terminal site.[19] This is due to the fact that weaker bases are more strongly influenced by the unfavorable charge distribution in the cage framework than are the adducts of stronger bases. In addition, the relative stability of the symmetric structure relative to the asymmetric structure is affected by the relative π bonding capacity of the ligand with the cage with an increase in π bonding favoring the symmetric structure. This trend has been observed experimentally in the order of the stabilities of the symmetric versus the asymmetric structure in the series $B_3H_7F^- > B_3H_8^- > B_3H_7NH_3$.[20] The observed bridged to terminal proton shift for **4** but not for **6** is therefore thought to arise primarily from a stabilization of the symmetric (bridged) structure by an increased π-bonding interaction between the cyclopentadienyl group in **6** relative to the primarily cage σ-bonded phosphorus atom in **4**.[20] Thus the ^{11}B NMR resonance for B(2) in **6** appears as a BH coupled doublet instead of the BH_2 coupled triplet observed for compound **4**. Several other metallapentaborane species, such as $[(\eta^5\text{-}C_5H_5)CoB_4H_8]$ (**9**) and $[2\text{-}(C_6H_6)RuB_4H_8]$ (**10**), have also

(17) Andrews, S. J.; Welch, A. J. *Acta Crystallogr. Sect. C: Cryst. Struct. Commun.* **1985**, *C41*, 1496.

(18) Emsley, J.; Hall, D. *The Chemistry of Phosphorus*; Wiley: New York, 1976.

(19) Kennedy, J. D. *Prog. Inorg. Chem.* **1984**, *32*, 519.

(20) Brown, L. D.; Lipscomb, W. N. *Inorg. Chem.* **1977**, *16*, 1.

Scheme II. Proposed Mechanistic Pathway for the Formation of Complex **4** from the Photoinduced Decarbonylation and Rearrangement Reaction of Complex **3**[a]

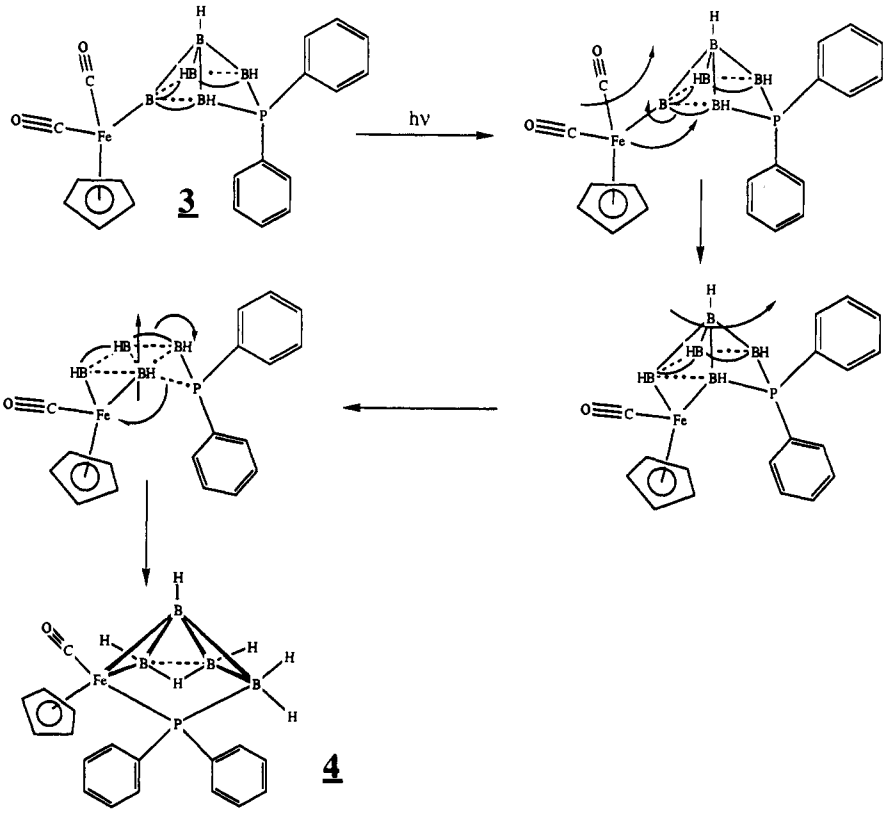

[a] Curved bonds indicate a bridging hydrogen atom.

been reported, but these compounds display structures which are based on a *nido*-B_5H_9 parent structure in which the metal fragment has substituted for a boron vertex in either the basal or apical positions.[4,5d,7,19]

The 80-MHz ^{11}B NMR spectrum of **4** consists of four resonances of equal intensity at 30.2, 25.7, −21.2, and −29.6 ppm. All the resonances are split into B–H coupled doublets except for the resonance at −29.6 ppm which appears as a pseudoquintet in the ^1H coupled spectrum. This latter coupling arises from the overlap of a B–P coupled doublet with the B–H coupled triplet of the BH_2 group. This assignment is confirmed in the ^1H decoupled spectrum in which all the ^{11}B resonances except the pseudoquintet collapse into singlets while the quintet collapses into the expected PB coupled doublet (J_{PB} = 80 Hz). The B–H triplet splitting of the BH_2 group of the pseudoquintet resonance in **4** is similar to that observed for the B(2) and B(5) atoms in the parent *arachno*-B_5H_{11} structure although the BH coupling constant for **4** is significantly less than that observed for *arachno*-B_5H_{11}.[21a,b] This attenuation of the coupling may indicate that there is some B–H–B bonding character remaining in this interaction.[21c] The 2D $\{^1H\}^{11}B$-^{11}B COSY NMR spectrum allows for the complete assignment of all the ^{11}B resonances. Cross peaks were clearly observed between the apical boron resonance (25.7 ppm) and all the other resonances except B(4), the basal boron atom attached to the iron center. The absence of this cross peak is expected, however, based upon the anticipated short T_1 relaxation times for both the B(1) and B(4) resonances (1.8 ms for the boron atom attached to the iron center versus an average of 8.9 ms for the other boron atoms in the starting complex **3**).[22] The combination of the two short T_1 times for these boron atoms would result in the absence of a cross peak in the spectrum. As expected, a cross peak was also missing between B(2) and B(4) but was present for the B(3) and B(4) interaction. The location of the resonance for the apical boron is shifted significantly downfield relative to comparable resonances for other related complexes.[5] The possibility of the structure of complex **4** being based upon a substituted *nido*-B_5H_9 parent structure, as in complexes **9** and **10**, can be eliminated primarily on the basis of electron counting and NMR data. Most metallapentaborane structures based on a substituted *nido*-B_5H_9 structure show either one type of boron (apical metal substitution) or two resonances (basal substitution) in the ^{11}B NMR spectrum. Complex **4**, however, clearly shows four well-separated ^{11}B NMR resonances. In addition, the 2D $\{^1H\}^{11}B$-^{11}B COSY NMR data and electron counting schemes for **4** described below do not support a substituted *nido*-B_5H_9 structure as the parent. The ^1H NMR for compound **4** shows, besides the typical resonances for the cyclopentadienyl and phenyl groups, a resonance for the single B–H–B bridging proton and a complex pattern for the terminal protons of the cage.[19] No resonances were found which corresponded to a M–H–B proton, as described above. In addition, no Fe–H–B stretch was observed in the FT-IR spectrum.

Electron counting according to Wade's rules[23] provides support for the structure of **4** as based on the *arachno*-B_5H_{11} parent structure. In this counting scheme, the $[(P(C_6H_5)_2R)(\eta^5\text{-}C_5H_5)(CO)Fe]$ (where R is the P–B cage attachment) fragment contributes five electrons to the cage bonding. This count arises from eight electrons from the iron atom, five from the cyclopentadienyl ring system, and two each from the carbonyl and phosphino groups for a total of seventeen electrons, twelve of which are involved in bonding the iron atom to its exopolyhedral ligand complement. Thus five electrons are contributed to the cage bonding from the iron fragment, six electrons are contributed from the three BH units, three electrons from the B(2) BH_2 unit,[23b]

(21) (a) Williams, R. E.; Gerhart, F. J.; Pier, E. *Inorg. Chem.* **1965**, *4*, 1239. (b) Eaton, G. R.; Lipscomb, W. N. *NMR Studies of Boron Hydrides and Related Compounds*; Benjamin: New York, 1969. (c) Todd, L. J.; Siedle, A. R. *Prog. NMR Spectrosc.* **1979**, *13*, 87.

(22) Part 5: Goodreau, B. H.; Spencer, J. T. *Inorg. Chem.* In press.

(23) (a) Wade, K. *Adv. Inorg. Chem. Radiochem.* **1976**, *18*, 1. (b) Shriver, D.; Atkins, P. W.; Langford, C. H. *Inorganic Chemistry*; Freeman: New York, 1990; p 354.

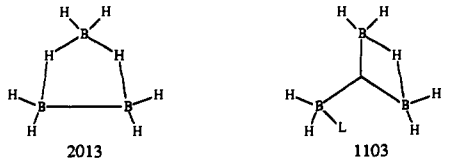

Figure 2. *Styx* topologies for 2013 and 1103 configuration for B_3-cage framework systems.[24]

one electron from the B–H–B bridging proton, and one electron from the bridging phosphorus atom for a total of sixteen skeletal electrons. The structure of complex **4**, with five vertices and a $2n + 6$ skeletal electron count, is thus expected to be based on an *arachno* five-vertex structure as proposed.

The formation of complex **4** from the photochemical irradiation of complex **3** is thought to proceed initially through the common organometallic decarbonylation reaction of the $Fe(\eta^5\text{-}C_5H_5)(CO)_2$ fragment. This proposed mechanistic pathway is shown in Scheme II. The decarbonylation reaction generates an unsaturated 16-electron iron center which then undergoes a shift from the terminal σ-bound species in **3** to an intermediate in which the iron fragment bridges boron vertices adjacent to the bridging diphenylphosphino group (B(3) and B(4)). This shift is favored over the possible shift to bridge the two boron atoms nonadjacent to the phosphorus atom (B(4) and B(5)) since the B(3) atom has a significantly greater electron density associated with it than does the B(5) atom, thus providing a greater stabilization of the 16-electron iron intermediate. A phosphorus atom shift to stabilize the 16-electron iron intermediate occurs with a concomitant apex boron elimination process. The tetraboron intermediate ultimately rearranges to maximize the P–Fe interaction to generate the observed structure of **4**. The shift of B(3) from a basal to an apical position is required to relieve the very large ring strain which results as a consequence of the formation of the strong iron–phosphorus bond. This final shift results in an apparent cage opening reaction and the formation of the observed *arachno* product. The final structure has a "saturated" 18-electron configuration around the iron center.

Compound **4** was found to be transformed into complex **5** by passage down a silica gel column. Recrystallization yielded a new complex **5** as a pure, air-stable, but slightly moisture sensitive material.

The proposed structure of compound **5**, shown in Scheme I, consists of a substituted *arachno*-B_4H_{10} parent structure[24] in which one vertex has been replaced by a $[(P(C_6H_5)_2R)(\eta^5\text{-}C_5H_5)(CO)Fe]$ fragment and one of the expected M–H–B bridging hydrogens has been replaced by a bridging $P(C_6H_5)_2$ group. In addition, as in complex **4**, the normally bridging hydrogen atom of the parent structure has shifted out to occupy a terminal position on the boron atom attached to the phosphorus center in complex **5**. As noted in the literature, although the structure of **5** can be thought of as based on the *arachno*-B_4H_{10} parent structure, the B_3H_7 fragment retains much of its incipient ligand character when coordinated to transition metals.[25,26] Thus, an alternate description for **5** is based on a metallated $B_3H_8^-$ structure in which the iron fragment coordinates to one boron atom of the $B_3H_8^-$ ligand through a Fe–H–B linkage and the phosphorus atom bridges between the iron and the adjacent boron atom in much the same fashion as a bridging M–H–B hydrogen atom. The structural assignment was confirmed by a single-crystal X-ray analysis of the complex. The molecular structure and numbering scheme for **5** is shown in Figure 3. In the structure, all the hydrogen atoms in the complex were located and refined without difficulty. Selected bond angles and bond lengths are given in Tables V and VI, respectively.

A number of metal complexes involving the triborane ligand fragment have been reported.[4,5b,27-48] Several features in the

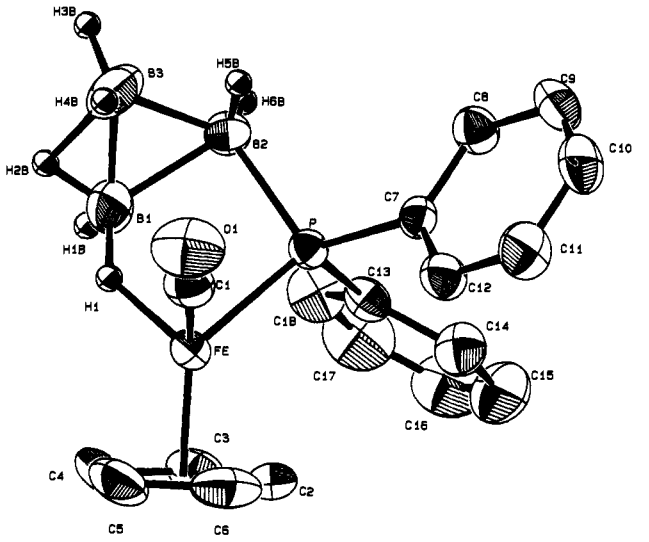

Figure 3. ORTEP drawing of $[Fe(\eta^5\text{-}C_5H_5)(CO)B_3H_7P(C_6H_5)_2]$ (**5**) showing the atomic numbering scheme. The thermal elipsoids are drawn at the 50% probability level. The hydrogen atoms on the C_6H_5 and C_5H_5 rings have been omitted for clarity.

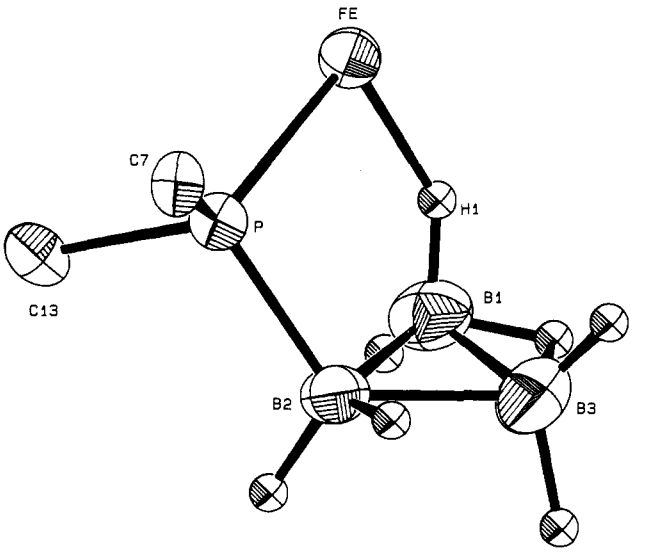

Figure 4. ORTEP drawing of $[Fe(\eta^5\text{-}C_5H_5)(CO)B_3H_7P(C_6H_5)_2]$ (**5**) showing the relative orientation of the B_3 cluster unit relative to the PR_2Fe fragment. The thermal elipsoids are drawn at the 50% probability level.

structure of **5** are particularly noteworthy, especially concerning the cage hydrogen atoms in **5** in comparison with other known

(24) Lipscomb, W. N. *Boron Hydrides*; Benjamin: New York, 1963.
(25) Housecroft, C. E.; Fehlner, T. P. *Inorg. Chem.* **1982**, *21*, 1739.
(26) Housecroft, C. E.; Owen, S. M.; Raithby, P. R.; Shaykh, B. A. M. *Organometallics* **1990**, *9*, 1617.
(27) Gaines, D. F.; Hildebrandt, S. J. *Inorg. Chem.* **1978**, *17*, 794.
(28) Hildebrandt, S. J.; Gaines, D. F.; Calabrese, J. C. *Inorg. Chem.* **1978**, *17*, 790.
(29) Haller, K. J.; Andersen, E. L.; Fehlner, T. P. *Inorg. Chem.* **1981**, *20*, 309.
(30) Andersen, E. L.; Haller, K. J.; Fehlner, T. P. *J. Am. Chem. Soc.* **1979**, *101*, 4390.
(31) Guggenberger, L. J.; Kane, A. R.; Muetterties, E. L. *J. Am. Chem. Soc.* **1972**, *94*, 5665.
(32) Kane, A. R.; Muetterties, E. L. *J. Am. Chem. Soc.* **1971**, *93*, 1041.
(33) Bould, J.; Greenwood, N. N.; Kennedy, J. D.; McDonald, W. S. *J. Chem. Soc., Dalton Trans.* **1985**, 1843.
(34) Greenwood, N. N.; Kennedy, J. D.; Reed, D. *J. Chem. Soc., Dalton Trans.* **1980**, 196.
(35) Klanberg, F.; Muetterties, E. L.; Guggenberger, L. J. *Inorg. Chem.* **1968**, *11*, 2272.
(36) (a) Lippard, S. J.; Melmed, K. M. *Inorg. Chem.* **1969**, *8*, 2755. (b) Brown, M.; Fontaine, L. R.; Greenwood, N. N.; MacKinnon, P.; Kennedy, J. D.; Thornton-Pett, M. *J. Chem. Soc., Dalton Trans.* **1987**, 2781.
(37) Bould, J.; Greenwood, N. N.; Kennedy, J. D. *J. Organomet. Chem.* **1983**, *249*, 11.
(38) Cooksey, B. G.; Gorham, J. D.; Morris, J. H.; Kane, L. *J. Chem. Soc., Dalton Trans.* **1978**, 141.

structures. First, the Fe–H bond distance in the Fe–H–B bridge (1.54 Å) is the shortest that has been reported for a triborane complex (M–H average = 1.74 Å). The Fe–B distance (2.53 Å), however, is the longest reported (M–B average = 2.28 Å with a range of 2.10 to 2.36 Å for first-row transition metals). Accompanying these structural features is a concomitant opening of the M–H–B bond angle from an average of 106.3° for known structures to 136° in **5**. This angle opening is presumably caused by the constraints imposed by the ring system formed from the relatively large $FePB_2H$ core, shown in Figure 4. The effect of the short Fe–H bond is seen in the ^1H NMR chemical shift for the M–H–B bridging hydrogen atom which is 6 ppm farther upfield in **5** than for any other M–H–B metallatriborane system. The structural and NMR data for this proton thus suggest that an increased metal hydride character should be associated with this bonding interaction, similar to other typical organometallic hydride complexes.[49] The position of H(5B), the hydrogen atom which has shifted to a terminal position from the bridging position of the parent compound, is also noteworthy. The B(3)–H(5B) and the B(2)–H(5B) distances (1.62 and 1.05 Å, respectively) clearly show the shift from the symmetrically bridged situation to the asymmetric terminally substituted relationship. The B_3-cage framework structure can thus be best described as a 1103 *styx* topology[19] rather than the 2013 topology reported for the $B_3H_8^-$ ligand and all reported metal triborane complexes (Figure 2).[24] Complex **5** represents the first structurally characterized metal triborane complex which exhibits a 1103 *styx* structure. This type of hydrogen asymmetry has been observed, although to a somewhat lesser degree than that observed in **5**, in the structure of $[Ph_3PCH_2B_3H_7]$ and other LB_3H_7 compounds (where L is a relatively weak donor ligand) in which the hydrogen arrangement has been described as a semibridging proton.[17] Calculations and NMR data, however, provide support for very little interaction between this hydrogen and the distant boron atom in $[Ph_3PCH_2B_3H_7]$.[50]

The metal bonding in **5** can be readily described by use of the effective atomic number (EAN) rule.[49] The iron center (8 electron core) achieves an 18-electron configuration through coordination to one CO ligand (2-electron donor), a cyclopentadienyl group (5-electron donor), a phosphorus ligand (2-electron donor), and the M–H–B interaction (1-electron donor). An alternative electron counting scheme, based on Wade's rules,[23] which focuses on the main group cluster, describes the system as containing 14 cage bonding electrons and is thus expected to display the observed *arachno* four-vertex structure.

The trend of B–B bond lengths in the triborane unit in **5** (B1–B2 > B2–B3 > B1–B3) is similar to that seen in several σ-substituted B_3 systems,[17,51,52] and the internal B–B–B angles (60.0° av in **5**) are nearly identical with those of the free $B_3H_8^-$ ligand (61°).[7d] The phosphorus atom is roughly tetrahedral with the bridging B–P–B angle of 89.7° in **3** opening to 103.6° for the B–P–Fe angle in **5**. The interplane angle between the B(1)–B(2)–B(3) and Fe–B(1)–B(2) planes of 113.8° is comparable with an angle of 124.5° reported from the electron on X-ray diffraction studies of *arachno*-B_4H_{10} and related compounds.[28,44,53] Other bond angles and distances in complex **5** are within the ranges typically observed for similar interactions in related complexes.

The ^{11}B NMR spectrum of compound **5** consisted of three resonances in a 1:1:1 relative ratio at 9.1, −24.4, and −38.5 ppm. The $B–H_{terminal}$ coupling for these resonances was not resolved and consisted of relatively broad, featureless peaks in the ^1H coupled spectra. This lack of resolution is unusual since other phosphorus-containing cluster species, in general, clearly show this coupling. In the case of the B(2) resonance, the lack of resolution is probably due to the complex overlap of a PB coupled doublet and the BH_2 coupled triplet.[54,55] The broad resonance at −24.5 ppm, however, did resolve to a phosphorus coupled doublet in the ^1H-decoupled spectrum. The 2D $\{^1H\}^{11}B$-^{11}B COSY NMR spectrum of **5** showed cross-peak connectivities consistent with the structure. In addition, both the one-bond PB and the two-bond PBB couplings were clearly resolved as 106 ($J_{PB(2)}$) and 18 Hz ($^2J_{PB(2)B(1)}$), respectively.[1,22] This is the first time "long-range" $^2J_{PBB}$ couplings have been observed for a borane cluster. Cross peaks were once again missing between the boron atom attached to the iron fragment and the other two borons due to the very short T_1 relaxation time for this boron as expected based on the spectra for complexes **3** and **4**. The ^1H NMR spectrum was as expected on the basis of the structure with the Fe–H–B resonance observed as a broad singlet at −21.3 ppm at room temperature. No variation in this resonance, except a slight sharpening of the spectrum at −20 °C, was observed over a wide range of temperatures.

The CO stretching frequency exhibited by complex **5** (1962 cm^{-1}) is at significantly lower frequency than the corresponding complex $[Fe(\eta^5\text{-}C_5H_5)(CO)B_3H_8]$, (**9**) (1995 cm^{-1}).[27] This can be attributed to the increase in the electron density on the iron center from the phosphorus ligand donation in complex **5**.

The structural and spectral relationships observed between complexes **4** and **5** provide additional strong support for the proposed assignment of the structure of complex **4**. The transformation of complex **4** into complex **5** with the loss of a vertex boron atom presumably results from the initial protonation of a cluster edge to form a Fe–H–B bridged arrangement. This process is in concept similar to the apical BH removal reaction by moderate bases, such as $Me_2NCH_2CH_2NMe_2$ (TMEDA), of *closo*-$M(R_2C_2B_4H_4)$ complexes to yield the *nido*-$M(R_2C_2B_3H_5)$ clusters.[6] No evidence was found in our work for the deprotonation of complex **4** by its passage down a silica gel column.

The elucidation of the proposed mechanistic pathways for the transformations described above and the study of further organometallic reaction and photochemistry of this interesting class of organometallic cluster compounds are currently in progress in our laboratory. These clusters are expected to allow for the observation of new structural types and reaction pathways not available for other classes of metallaborane complexes through the stabilization of reaction intermediates by the heteroatom such as described in this paper. Insights into these processes are critical to the application and understanding of the reaction chemistry of other organometallic and borane cluster species.

Acknowledgment. We thank the National Science Foundation (Grant No. MSS-89-09793), the National Science Foundation Research Experiences for Undergraduates Site Award (Grant No. CHE-8900471), the donors of the Petroleum Research Fund, administered by the American Chemical Society, the Wright-Patterson Laboratory (Award No. F33615-90-C-5291), and the Industrial Affiliates Program of the Center for Molecular Electronics for support of this work. We also thank Mr. Terry O'Connell for his generous assistance in obtaining the high-resolution mass spectral data.

(39) Borlin, J.; Gaines, D. F. *J. Am. Chem. Soc.* **1972**, *94*, 1367.
(40) Chen, M. W.; Gaines, D. F.; Hoard, L. G. *Inorg. Chem.* **1980**, *19*, 2989.
(41) Guggenberger, L. J. *Inorg. Chem.* **1970**, *9*, 367.
(42) Housecroft, C. E. *Inorg. Chem.* **1986**, *25*, 3108.
(43) Greenwood, N. N.; Kennedy, J. D.; Thornton-Pett, M.; Woollins, J. D. *J. Chem. Soc., Dalton Trans.* **1985**, 2397.
(44) Dain, C. J.; Downs, A. J.; Rankin, D. W. H. *J. Chem. Soc., Dalton Trans.* **1981**, 2465.
(45) Muetterties, E. L.; Peet, W. G.; Wegner, P. A.; Alegranti, C. W. *Inorg. Chem.* **1970**, *9*, 2447.
(46) Lippard, S. J.; Ucko, D. A. *Inorg. Chem.* **1968**, *7*, 1051.
(47) Gaines, D. F.; Hildebrandt, S. J. *J. Am. Chem. Soc.* **1974**, *96*, 5574.
(48) Klanberg, F.; Muetterties, E. L. *J. Am. Chem. Soc.* **1968**, *90*, 3296.
(49) Collman, J. P.; Hegedus, L. S.; Norton, J. R.; Finke, R. G. *Principles and Applications of Organotransition Metal Chemistry*; University Science: Mill Valey, CA, 1987.
(50) Glass, J. A., Jr.; Whelan, T. A.; Spencer, J. T. *Organometallics* **1991**, *10*, 1148.
(51) Nordman, C. E.; Reimann, C. *J. Am. Chem. Soc.* **1959**, *81*, 3538.
(52) Andrews, S. J.; Welch, A. J. *Inorg. Chim. Acta* **1984**, *88*, 153.
(53) Chen, M. W.; Calabrese, J. C.; Gaines, D. F.; Hillenbrand, D. F. *J. Am. Chem. Soc.* **1980**, *102*, 4928.
(54) (a) Miller, R. W.; Donaghy, K. J.; Spencer, J. T. *Organometallics* **1991**, *10*, 1161. (b) Miller, R. W.; Donaghy, K. J.; Spencer, J. T. *Phosphorus, Sulfur and Silicon* **1991**, *57*, 287.
(55) Burg, A. B.; Heinen, H. *Inorg. Chem.* **1968**, *7*, 1021.

Supplementary Material Available: Tables of complete crystallographic data, all atom coordinates including all hydrogen atoms, anisotropic thermal parameters, bond distances and angles involving both non-hydrogen and hydrogen atoms, intermolecular distances, and selected dihedral angles between least-squares planes and PLUTO steropair and packing diagrams for **5** (35 pages); a listing of observed and calculated structure factors (17 pages). Ordering information is given on any current masthead page. A complete listing of previously reported transition metal B_3 complexes is also available from the author.

An NMR Investigation of the Interactions Occurring between Peroxovanadates and Peptides

Alan S. Tracey* and Jaswinder S. Jaswal

Contribution from the Department of Chemistry, Simon Fraser University, Burnaby, B.C. V5A 1S6, Canada. *Received June 24, 1991*

Abstract: ^{51}V nuclear magnetic resonance has been used in the investigation of the reactions which occur between peroxovanadates and simple peptides and other small molecules in aqueous solution. Variation of the concentration of the reactants and changes in the pH of the solutions allowed product stoichiometry, protonation states, and equilibrium constants to be determined. It was found that the diperoxovanadate $VO(OO)_2(H_2O)_2^-$ readily formed monodentate complexes with both the amino and carboxylate functionalities of the peptides. A linear free energy relationship between the formation constants of the products and the pK_a values of the conjugate acids of the reactant groups was observed. This relationship showed that product formation was favored by stronger electron-donating ligands. Inhibition of the vanadate-catalyzed decomposition of hydrogen peroxide by peptides was studied by ^{51}V NMR and UV spectroscopy. The results were consistent with the formation of a monoperoxopeptidovanadate as the inhibiting species. It was found that the terminal amino and carboxylate functionalities and an amide N-H in the peptide bond were all required for the peptide-induced inhibition to occur. The relevance of these results to some aspects of the biochemical function of peroxovanadates is discussed.

Introduction

It has been known for many years that vanadium oxoanions give rise to many biological responses.[1] Many of these responses have their origin in the activation or inhibitions of the function of a number of different enzymes. It is becoming increasingly clear that (oxo)peroxovanadium(V) anions similarly generate a number of biological and biochemical responses. These responses include the following: activation of the insulin receptor[2] and other tyrosine kinases;[3] enhanced binding of insulin-like growth factor II receptor binding to adipocytes;[4] mediation of Na^+ transport by (Na^+, K^+) ATPase;[5] and antitumor activity.[6]

The molecular mechanisms by which these responses are generated are not known, nor is there sufficient evidence available to make a credible hypothesis. Several processes which might lead to the observed biochemical responses come readily to mind. Peroxovanadates might directly activate or inhibit the enzymic system responsible for the observation or may give rise to covalent modification of the proteins by promoting oxidation, thus influencing the function of the system. An additional possibility is that peroxovanadate might provide a "slow-release" mechanism, enhancing the concentration of vanadate in locations not otherwise readily accessible. In this case vanadate would generate the observed response. Alternate possibilities certainly exist.

The identification of the actual processes involved requires an understanding of the basic chemistry of peroxovanadates, in particular their interactions with amino acids, peptides, other metabolites and small molecules. In order to address these problems we have recently initiated a study of the formation of peroxovanadium(V) complexes and the subsequent reactions of these materials.

The chemistry of the vanadate/peroxide system can be quite complex since vanadate in the presence of hydrogen peroxide forms a number of products, their relative concentrations being dependent on vanadate and peroxide concentration and on pH.[7-11] However, at near neutral pH and with concentrations of a few millimolar for both reactants, the predominant products are the mono-, di-, and triperoxovanadates and the tetraperoxodivanadate.[9] All of the above materials are of interest and a study of their reactions with some simple di- and tripeptides and related molecules is reported here.

The study of the chemistry of the peroxovanadates is often complicated by the vanadate-catalyzed disproportionation of hydrogen peroxide to oxygen and water. This topic has been recently reviewed and the mechanism of action discussed.[12] Fortunately, this decomposition does not present a serious problem for this study since the decomposition is slow relative to the time taken to finish the experiments. Furthermore, many of the ligands utilized in this study strongly inhibit the disproportionation.

Experimental Section

Materials. All reagents, unless mentioned otherwise, used in this study were reagent or higher quality materials purchased from major suppliers. Of note in this regard is that vanadium(V) oxide 99.99% was purchased form Aldrich Chemical Co. and hydrogen peroxide from Fischer Scientific Co. The peptides were obtained from Sigma Chemical Co. Proton NMR spectra were obtained for the peptides and other ligands of this study, as deemed necessary. All were used as supplied. Glycylglycyl-

(1) *Vanadium in Biological Systems*; Chasteen, N. D., Ed.; Kluwer Academic Publishers: Dordrecht, Boston, London, 1990.
(2) Fantus, I. G.; Kadota, S.; Deragon, G.; Foster, B.; Posner, B. I. *Biochemistry* **1989**, *28*, 8864-8871.
(3) Heffetz, D.; Bushkin, I.; Dror, R.; Zick, Y. *J. Biol. Chem.* **1990**, *265*, 2896-2902.
(4) Kadota, S.; Fantus, G.; Deragon, G.; Guyda, H. J.; Posner, B. I. *J. Biol. Chem.* **1987**, *262*, 8252-8256.
(5) Jakubowski, J.; Jakob, A. *Eur. J. Biochem.* **1990**, 541-549.
(6) Djordjevic, C.; Wampler, G. L. *J. Inorg. Biochem.* **1985**, *25*, 51-55.
(7) Harrison, A. T.; Howarth, O. W. *J. Chem. Soc., Dalton Trans.* **1985**, 1173-1175.
(8) Campbell, N. J.; Dengel, A. C.; Griffith, W. P. *Polyhedron* **1989**, *8*, 1379-1386.
(9) Jaswal, J. S.; Tracey, A. S. *Inorg. Chem.* **1991**, *30*, 3718-3722.
(10) Souchay, P.; Chauveau, F. *C. R. Hebd. Seances Acad. Sci.* **1957**, *245*, 1434-1436.
(11) Chauveau, F. *Bull. Soc. Chim. Fr.* **1960**, 819-833.
(12) Butler, A. *Vanadium in Biological Systems*; Chasteen, N. D., Ed.; Kluwer Academic Publishers: Dordrecht, Boston, London, 1990; pp 25-49.

0002-7863/92/1514-3835$03.00/0